Influence of bed material size heterogeneity on bedload transport uncertainty

Li Chen[1] and Mark C. Stone[1]

Received 1 September 2006; revised 20 August 2007; accepted 21 September 2007; published 4 January 2008.

[1] The bed material grain size distribution of gravel bed streams is often spatially heterogeneous. The heterogeneity is actually a random parameter, even for a ''well-mixed mixture,'' which potentially causes the transport rate for a given bed material to become an uncertain variable. The cause of bed material heterogeneity is the nonuniformity of the bed material, which is analyzed in this paper using examples from field observations and experimental data. The Monte Carlo simulation method is applied to study the uncertainty of the bedload transport rate using Wilcock's experimental data (P. R. Wilcock et al., 2001; P. R. Wilcock and J. C. Crowe, 2003). Each realization of the Monte Carlo simulation employed a randomly generated grain size distribution field for the entire simulation domain. With sufficient realizations the simulation results were adequate to show that the transport rates were a random variable and the mean transport rates did not fall on a single-valued curve when the local heterogeneity was taken into account. The results indicate that the bedload transport rate of nonuniform sediment has an intrinsic uncertainty that can result solely from the bed material. The results also partially account for the scatter of the fractional transport rate within Wilcock's experimental data. This study presents an important concept in understanding the uncertainty associated with estimates of sediment transport.

Citation: Chen, L., and M. C. Stone (2008), Influence of bed material size heterogeneity on bedload transport uncertainty, *Water Resour. Res.*, *44*, W01405, doi:10.1029/2006WR005483.

1. Introduction

[2] The transport of coarse sediment as bedload is important for the evolution of channel morphology, especially in mountain streams. However, understanding of this complex sediment transport process remains poor. The physical process involves cycles of particle entrainment, movement along the stream (which includes rolling, sliding, and saltation) and deposition on the bed. The transport of particles is controlled by the interaction of highly turbulent flow with stationary and moving particles. For nonuniform sediments, this process is further complicated by the interaction between size fractions.

[3] A number of physically based models of particle entrainment and transport have been developed on the basis of comprehensive force balance analyses [*Bagnold*, 1966; *Yalin*, 1977; *Wiberg and Smith*, 1989; *Bridge and Bennett*, 1992]. Because of the complexity of forces acting on particles, quantifying this condition is inexact. Therefore the final equations of bedload transport models depend on several unknown parameters which need to be determined through experimental data.

[4] Stochastic approaches have gained attention as a method to account for uncertainty in the bedload transport process. *Einstein* [1950] offered a stochastic model by introducing a probability function to describe incipient particle motion. This probability is usually determined by the instantaneous shear stress distribution, which is assumed to follow a normal or lognormal probability density function (PDF). Though this method is theoretically closer to reality, it still depends on several undetermined parameters. To date, very limited work has been completed on the issue of nonuniform sediments. The similarity method is most widely used by researchers when handling nonuniform bed material [e.g., *Parker et al.*, 1982; *Parker*, 1990; *Wilcock and Crowe*, 2003]. This method starts directly from observed data. Nondimensional similarity variables are then adopted to collapse the data sets for all size fractions. Finally, the hiding exposure function is proposed to account for the interaction between different size fractions and to reach perfect similarity. All of these models require reliable bedload transport measurements for model parameterization and calibration.

[5] Though a number of field observations and flume experimental results are available, it is difficult to find good data sets to calibrate bedload transport models. For mechanism analyses, flume experimental data are usually preferred over field observations because researchers have more control over flow properties and bed materials. Field observations typically include many complicating factors that affect the quality of the data. For example, flow conditions are difficult to measure with high accuracy and in short periods of time and the flow field often deviates from steady state conditions; the channel cross-section geometry often affects the transport rate if the unit width transport rate is used to derive a transport equation; and the transport process may not reach equilibrium in the field because of varying flow conditions and bed material varia-

[1]Division of Hydrologic Sciences, Desert Research Institute, Las Vegas, Nevada, USA.

0043-1397/08/2006WR005483$09.00

tions. Another practical difficulty is the measurement of bed material grain size distributions (GSD). Also, practical considerations in field sampling techniques limit data quality and availability, particularly in deep- or high-velocity flows [*Stone and Hotchkiss*, 2007a]. Because of these difficulties, scatter in observational data is often attributed to technical limitations and the complexity of natural systems.

[6] A carefully designed flume experiment can avoid most of the aforementioned difficulties and provide a more comprehensive data set. Such a data set was produced by Wilcock and others [*Wilcock and McArdell*, 1993; *Wilcock et al.*, 2001] through a series of bedload transport experiments that carefully measured a number of flow and sediment variables including flow depth and velocity, surface and substrate bed material composition, and water surface slope. A range of bed material mixtures and flow conditions were used over 47 experimental runs; providing a comprehensive collection of observations for the main variables of concern. The experiments covered a range of bed material particle sizes (0.2–64 mm), Reynolds numbers (25,000–115,000), and shear stresses (2.78–23.6 N/m^2). With such an extensive experimental design, Wilcock's work produced a useful data set for improving our understanding of bedload transport.

[7] On the basis of their experimental data, *Wilcock et al.* [2001] and *Wilcock and Crowe* [2003] developed a bedload transport model based on the similarity collapse method, which is widely adopted in bedload transport studies. Following the similarity treatment, the data set displayed a clear trend and the model described this trend fairly well. However, although the model reproduced the experimental data well for the total transport rate, the data displayed noticeable scatter for the fractional transport rate (Figures 1a and 1b). The nondimensional transport rate has a vertical belt width of 1–2 orders of magnitude, illustrating considerable uncertainty. The uncertainty was observed to increase as the normalized shear stress (ϕ_i) decreased. Such uncertainty is notable for a well controlled flume experiment with reliable measurements. It is unlikely that turbulence was the dominant cause for the observed transport uncertainty. Turbulent fluctuations in near-bed velocity and shear stress are known to cause fluctuations in sediment entrainment and transport rates [*Papanicolaou et al.*, 2001; *Wu and Jiang*, 2007]. However, turbulence is a quasi-periodic process with a much higher frequency than the experimental duration used by Wilcock [*Stone and Hotchkiss*, 2007b]. Therefore the transport rate uncertainty caused by turbulence should largely be removed from the time averaged results. According to Wilcock's similarity analysis, it is hard to substantially improve the similarity of the normalized data set. Thus the cause of the uncertainty is likely related to the sediment itself. The fact that the model describes the total transport rate better than the fractional transport rates implies that the nonuniform GSD could be an important factor contributing to the uncertainty. Nonuniform sediment transport has been investigated by many researchers and the influence of nonuniformity on uncertainty is supported by the results from previous studies. For example, a comparison between Figures 1c and 1d [from *Chien and Wan*, 1999] for laboratory experiments reveals that higher variations in bedload transport rates were observed for the case of nonuniform sediments when compared to uniform sediments. The work presented here investigates the impact of the heterogeneity of the local GSD on the uncertainty in bedload transport rates. In the literature, the term sediment heterogeneity is often used synonymously with the term nonuniform sediment [e.g., *Bridge and Bennett*, 1992]. In this study, sediment heterogeneity describes spatially varying local GSD.

[8] Section 2 of this paper examines the phenomenon of GSD heterogeneity using examples from field observations and laboratory experiments. The conditions required to define heterogeneity are discussed and the physical property of heterogeneity is examined through a Probability Density Function of the GSD, which provides the foundation for the following stochastic analysis. Wilcock and Crowe's bedload transport model [*Wilcock and Crowe*, 2003] that will be used in the heterogeneity study is shortly summarized in section 3. In section 4, Wilcock's experimental data are reanalyzed through a Monte Carlo simulation approach with randomly generated particle distributions, which all match the global GSD. The Monte Carlo simulation results are then used to investigate the impacts of sediment heterogeneity on bedload transport rates. Sections 5 and 6 contain discussions of results and implications respectively.

2. Heterogeneity of the Local Grain Size Distribution

[9] An implicit assumption made in bedload transport studies for nonuniform bed material is that the bed material is nonuniform but homogeneous. This implies that the size distribution is the same everywhere within the study domain. In the mixture of nonuniform bed materials, every particle is surrounded by neighbor particles. The particles interact with each other and induce the hiding and exposure effect. Because of this effect, each size fraction has a different transport rate from that of a uniform material with the same size. Transport rates are studied by size fractions for nonuniform sediment. Usually a particle size composition representing the whole domain is adopted for the transport rate study (henceforth referred to as the global GSD). Local conditions, however, can vary significantly from the global GSD, introducing the effect of heterogeneity of the local GSD.

[10] The gravel bed GSD provided in experimental or field observation data sets is typically sampled from small areas on the bed to represent a large area. This is to approximate the statistical average value of the GSD for the entire study domain, the global GSD. The local GSD could be different from this average, even for a "well mixed mixture" as demonstrated below using Wilcock's experimental data. If the study domain is divided into subareas, particles of each size fraction may not be evenly distributed in each subarea, provided the number of subareas is comparable with the number of large size particles in the study domain. This effect is more significant if the mixture of bed material contains a wide range of particle sizes. The result of this effect is that the transport rate in each subarea is not equal to the average transport rate for the whole study area. Therefore the predicted total transport rate by averaging the transport rates of subareas may not be equal to the predicted transport rate by using the global GSD. This means that the transport rate could be an uncertain variable

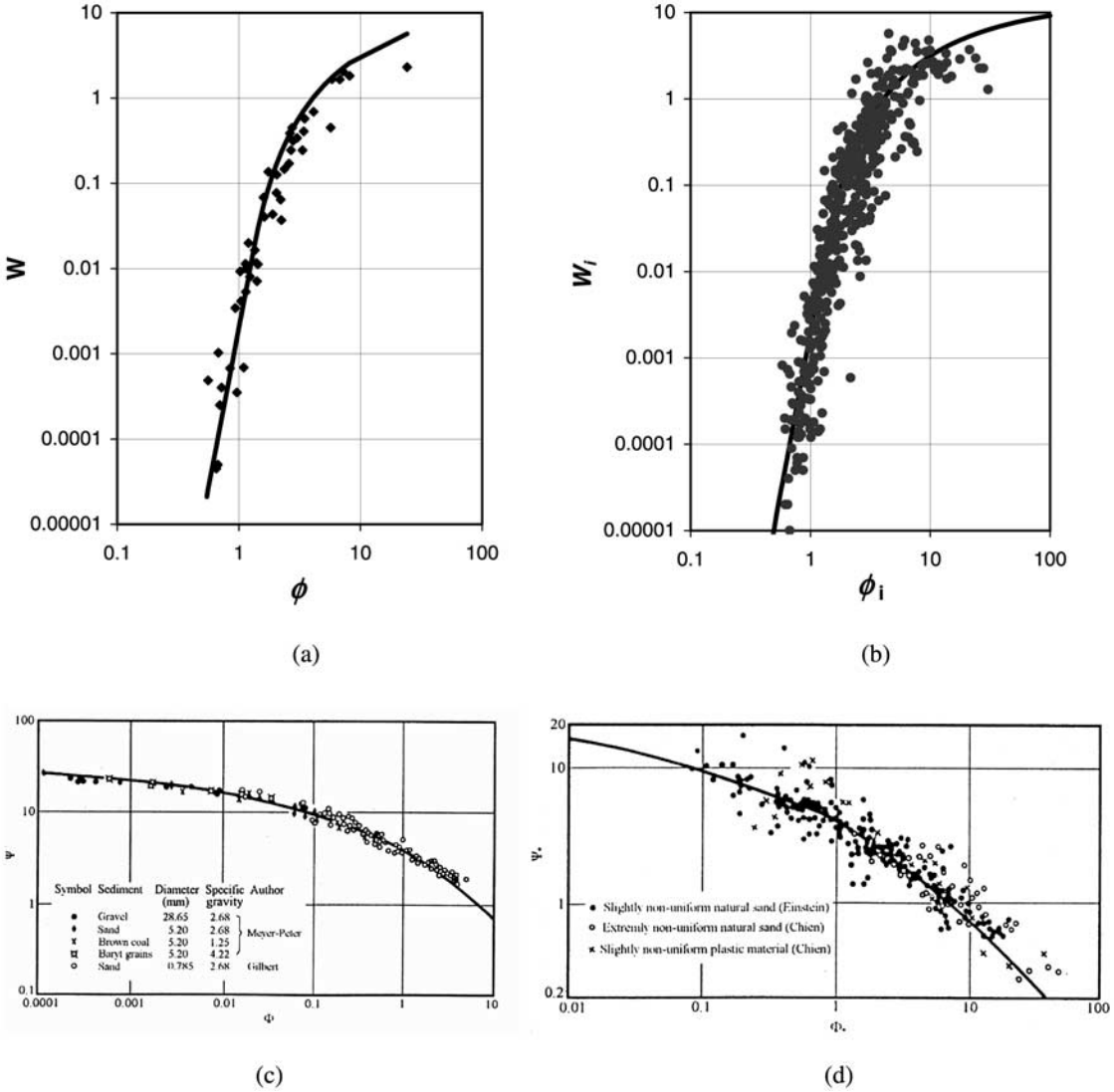

Figure 1. (a) and (b) Dimensionless total transport rate W and fractional transport rate W_i as functions of dimensionless shear stress φ (φ_i), using Wilcock's experimental data [*Wilcock et al.*, 2001; *Wilcock and Crowe*, 2003]. The geometric mean size of bed material is used for the dimensionless shear stress. The solid curves are the Wilcock and Crowe equation. (c) and (d) A comparison of uniform and nonuniform bedload transport data. These graphs are adapted from *Chien and Wan* [1999, Figures 9.14 and 9.25] (with permission from the American Society of Civil Engineers). The solid curves are Einstein's bedload transport function. Parameters Φ and Ψ, defined in Einstein's function, are the nondimensional bedload transport rate and the reciprocal of nondimensional flow shear stress.

rather than a fixed value because of the uncertain local GSD.

2.1. Examples of the Heterogeneity of Grain Size Distributions

[11] The heterogeneity of grain size distributions can be visually observed in many sites and has been noted in previous studies [e.g., *Seal and Paola*, 1995]. To illustrate the heterogeneity of GSDs in natural streams, we collected bed material samples from seven random locations within a 10 meter reach of Willow Creek, a gravel bed stream in the Spring Mountains of Nevada. On the basis of visual observations, the global distribution of bed materials in the 10 m reach appeared to be nearly homogeneous with a few large size cobbles (>64 mm in diameter) showing local heterogeneity. Because of shallow flows, a fairly high amount of small particles, the lack of a defined armor layer, and the very shallow flow depth (less than 10cm) a volumetric sampling technique was employed. Following the techniques described by *Bunte and Abt* [2001], volumetric samples were collected with a shovel and transferred to buckets at seven sampling stations within a 20 cm by 20 cm region of the streambed. The samples were transferred to the laboratory and the GSDs were determined using a standard sieve analysis. The results, shown in Figure 2, illustrate the heterogeneity of the local GSD. The median particle size (d_{50}) varied from 13.9 mm to 58.1 mm and the geometric mean size (d_m) ranged from 13.5 mm to 35.4 mm. This simple exercise demonstrates that substantial

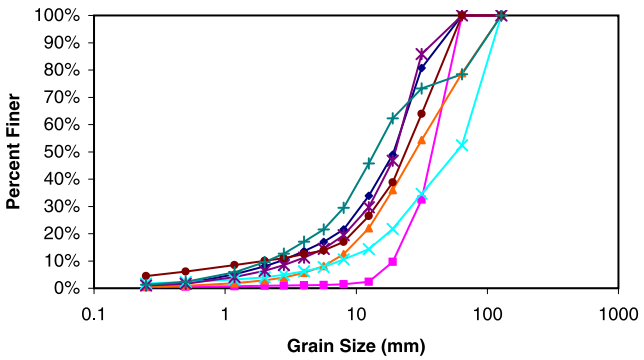

Figure 2. Grain size distribution of seven samples collected from Willow Creek, a gravel bed stream in Nevada. Samples show significant spatial heterogeneity.

heterogeneity in the GSD can exist within an apparently homogenous stream reach.

[12] Wilcock's gravel-sand mixture experiment also illustrates the nature of bed material heterogeneity. Even without visual observations of the bed material, the heterogeneity of bed material may be elucidated through a more detailed analysis on the GSD. The bed material mixture consisted of particles ranging from very coarse gravel to very fine sand. For example, the BOMC6 case had the surface GSD listed in Table 1. In this table, the first column shows the sieve sizes, the second column shows the geometric mean sizes for each fraction, and the third column contains the percent mass for each size fraction.

[13] To illustrate the concept of particle size heterogeneity, it is convenient to calculate the minimum required area of the surface layer that contains exactly this GSD. We still use experiment BOMC6 as the example. For simplicity, the following assumptions are made: (1) particles are all spherical; (2) particles in each size fraction are uniform and the representative size is the geometric mean size of this fraction; and (3) the porosity of the mixture is 0.3 everywhere.

[14] Table 2 shows the computation of the minimum required volume, V_{min}, that has the global GSD. Each subarea of the mixture that contains exactly this size composition should have an integer number of the largest

Table 1. Particle Size Distribution in Wilcock's Experiments

Diameter, mm		
Size Fraction	Geometric Mean	Percentage of Weight, %
64–45.3	53.84	2.5
45.3–32	38.07	2.7
32–22.6	26.89	8.2
22.6–16	19.02	8.1
16–11.3	13.45	5.6
11.3–8	9.51	4.6
8–5.66	6.73	5.6
5.66–4	4.76	5.6
4–2.83	3.37	6.4
2.83–2	2.38	1.9
2–1.41	1.68	3.3
1.41–1	1.19	5.6
1–0.5	0.71	19.4
0.5–0.21	0.32	20.5

Table 2. Example Calculation of Bed Material Heterogeneity[a]

d_k, mm	p_k	V_k, mm^3	G_k	Integer G_k	Total V_k, m^3
53.844	0.025	81735.47	1	1	8.17E-05
38.074	0.027	28899.09	3.055	3	8.67E-05
26.892	0.082	10182.82	26.33	26	2.65E-04
19.016	0.081	3600.44	73.55	74	2.66E-04
13.446	0.056	1272.85	143.84	144	1.83E-04
9.508	0.046	450.06	334.17	334	1.50E-04
6.729	0.056	159.53	1147.65	1148	1.83E-04
4.758	0.056	56.40	3246.29	3246	1.83E-04
3.365	0.064	19.95	10488.10	10488	2.09E-04
2.379	0.019	7.05	8811.35	8811	6.21E-05
1.679	0.033	2.48	43534.52	43535	1.08E-04
1.187	0.056	0.876	209077.75	209078	1.83E-04
0.707	0.194	0.185	3427799.62	3427800	6.34E-04
0.324	0.205	0.0178	37634900.2	37634900	6.70E-04

[a] $V_{min} = \sum V_k/(1 - P) = 0.0047$ m^3.

particle (i.e., at least one 53.84 mm gravel particle in Wilcock's BOMC6 case). The procedure in Table 2 to calculate the V_{min} is: 1) with the mean size (d_k), the percentage (p_k) and the single particle volume V_k of size fraction k, the particle number particle number G_k (using $G_1 = 1$) is calculated; 2) G_i is rounded to an integer and used to calculate the total volume for size fraction k; 3) then the total volume of the mixture V_{min} for BOMC6 can be calculated using Table 2, which shows:

$$V_{min} = \sum_{k=1}^{m} G_k V_k/(1-p) = 0.0047 \text{ m}^3 \quad (1)$$

Where p is the porosity. If the surface layer thickness is defined as the mean size of the largest size fraction (53.84 mm in this case), the sideline length of a square area of such a volume in the surface layer is:

$$L_{min} = 0.3 \text{ m} \quad (2)$$

This happened to be one half of the width of Wilcock's experimental flume. If we define the smallest covering area as:

$$A_{min} = L_{min}^2 \quad (3)$$

a consequence is that the "well-mixed mixture", or the homogeneous bed material, should describe an area much larger than A_{min}, or a spatial scale much larger than L_{min}. For an area smaller than this scale, the global GSD does not exist.

[15] However, in an area containing the global GSD, particles may not interact over the entire domain. In other words, one particle cannot influence other particles that are too distant. Therefore the actual hiding and exposure effect may not occur for the global GSD and the local GSD must be considered. For a spatial scale on the same order of A_{min} or smaller, the GSD becomes heterogeneous. In the case of Wilcock's BOMC6 experiment, L_{min} is of the same order as the channel width. This implies that the heterogeneity of the GSD is not a second-order effect, and thus it is not negligible.

[16] In the above calculation, the surface layer thickness value adopted is the largest possible value, which was defined as D_{90} by *Parker et al.* [1982]. In addition, the real porosity value is generally larger than 0.3, as used here. However, these were conservative estimates intended to avoid overestimation of $A_{\min}$ which would exaggerate the heterogeneity effect.

2.2. Probability Density Function of Grain Size Distributions in a Mixture

[17] When the local GSD is accounted for, the transport rate problem for heterogeneous bed material can be defined as follows. The study area A is a bed area no less than the smallest area $A_{\min}$ that is able to contain the same size fraction composition as the entire bed surface. If A is divided into n subareas, each subarea contains m size fractions, and the percentage of each size fraction is $p_{i,k}(i = 1, \ldots, m, k = 1,\ldots, n)$, then the whole area averaged percentage of each size fraction is $\overline{p_i}$. Because the size composition is a stochastic variable, the goal of the solution is to seek the expression of the probability density function $f(p_{i,k})$ in order to find the size composition in different subareas which satisfies the following constraint conditions:

$$\sum_{i=1}^{m} p_{i,k} = 1 \tag{4}$$

$$\frac{1}{n}\sum_{k=1}^{n} p_{i,k} = \overline{p_i} \tag{5}$$

The first constraint condition shows that probability density functions for each size fraction are actually correlated with each other.

[18] The distribution function, $f(p_{i,k})$, however, is difficult to determine because of the correlation between size functions. If only the second constraint condition is considered (i.e., each size fraction is calculated separately), the probability of K out of T_i particles in one subarea can be expressed with a binomial distribution:

$$p(T_i, K) = \binom{T_i}{K} R^K (1-R)^{T_i - K} \tag{6}$$

where T_i is the total number of the ith size fraction particle, and R is the probability of a particle falling into one subarea, $R = 1/n$. The percentage of each size fraction is then calculated as:

$$p_{i,k} = p(T_i, K) \bullet \frac{KV_i}{(1-P)V} = \binom{T_i}{K} R^K (1-R)^{T_i - K} \bullet \frac{KV_i}{(1-P)V} \tag{7}$$

Where V_i is the volume of one single particle of the *ith* size fraction, V is the volume of the kth subarea, and P is porosity. When T_i is a large number, this distribution of particle numbers could be approximated by a normal distribution based on (6)

$$f[p(T_i, K)] = \frac{1}{\sqrt{2\pi T_i RS}} \exp\left[-\frac{(K - T_i R)^2}{T_i RS}\right] \tag{8}$$

where, $S = 1-R$, T_iR is the mean and T_iRS is the variance of the distribution. If T_i is a large number (i.e., for fine size fractions), the ratio $\sqrt{TiRS}/T_iR$ is small, which means the distribution is mainly concentrated in a relatively narrow range around the mean value. Thus the spatial distribution of particle numbers is close to uniform. This encourages us to make an assumption that, when considering all constraint conditions, the ratio of particle numbers of two fine size fractions is spatially invariant, i.e.,

$$\frac{G_{i,k_1}}{G_{j,k_1}} = \frac{G_{i,k_2}}{G_{j,k_2}} \tag{9}$$

where $G_{i,k1}$ and $G_{j,k2}$ are grain size percentages of fine size fractions i and j in subareas k_1 and k_2. This equation allows us to achieve a well-mixed mixture with the following physical procedure: (1) randomly place coarser fraction particles into each cell without considering the first constraint condition, and (2) use well-mixed finer fractions to fill every cell to the same cell volume. This approach will be used in the stochastic simulation below.

3. Wilcock and Crowe Model

[19] In the following section the impact of a heterogeneous GSD on the transport rate will be examined. In this section we describe the bedload transport model presented by *Wilcock and Crowe* [2003]. The regressive model was established from a similarity collapse of the aforementioned data set. In this study, it is assumed that the model predicts the accurate fractional transport rate for any possible bed material GSD in a small subarea. The model is summarized as follows:

$$W_i = \begin{cases} 0.002\phi_i^{7.5} & \text{for } \phi_i < 1.35 \\ 14\left(1 - \frac{0.894}{\phi_i^{0.5}}\right)^{4.5} & \text{for } \phi_i \geq 1.35 \end{cases} \tag{10}$$

where $W_i = \dfrac{(s-1)gq_{bi}}{P_i u_*^3}$ is the nondimensional transport rate of ith size fraction, $\phi_i = \tau/\tau_{ri}$ is the nondimensional shear stress; q_{bi} is the volumetric transport rate per unit width of ith size fraction; $s = \rho_s/\rho$ is the ratio of sediment to water density; g is gravitational acceleration; P_i is the percentage of the ith size fraction in bed surface; u_* is shear velocity;τ is bed shear stress; τ_{ri} is the reference value of τ which is calculated with a hiding function:

$$\frac{\tau_{ri}}{\tau_{rm}} = \left(\frac{D_i}{D_{sm}}\right)^b \tag{11}$$

and

$$b = \frac{0.67}{1 + \exp\left(1.5 - \frac{D_i}{D_{sm}}\right)} \tag{12}$$

in which

$$\tau_{rm}^* = \frac{\tau_{rm}}{(s-1)\rho g D_{sm}} \tag{13}$$

$$\tau_{rm}^* = 0.021 + 0.015\exp(-20F_s) \tag{14}$$

where D_{sm} is geometric mean size of bed surface; τ_{rm} is the shear stress for D_{sm}; τ^*_{rm} is Shields parameter, and F_s is the percentage of sand in the bed surface.

[20] In the Wilcock and Crowe model, the interaction between particles of different sizes is accounted for with a hiding function. This increases the mobility of coarse particles and reduces the mobility of fine particles when compared with the corresponding uniform bed material of the same size. *Wilcock et al.* [2001] also found that the gravel transport rate is sensitive to the total sand content percentage. The key parameters of the hiding function are the geometric mean size and sand content.

4. Monte Carlo Simulation

[21] In this section, we examined the difference between the transport rate averaged from subareas with local GSD and the transport rate calculated with the global GSD. To study the impact of GSD heterogeneity, the local GSD for each subarea is needed. Wilcock's experimental data were used in this study to provide the hydraulic conditions, the dimensions of the domain, and the global GSD. However, for a given global GSD, the local GSD in each subarea is uncertain because the particle allocation is random. This uncertainty should be accounted for in order to obtain an averaged effect of the heterogeneity. Since it is impossible to consider every possible distribution in each local subarea, the Monte Carlo method was employed for this study.

[22] The Monte Carlo simulation is a widely used computational method for stochastic processes. Unlike deterministic methods, the Monte Carlo simulation can provide a series of possible values for variables of concern, which allows the modeler to investigate the resulting distribution caused by these variables. In this study, the Monte Carlo approach was employed in a sequence method. A series of realizations for bedload transport were simulated separately in order to obtain a sequence of bedload transport rates. In each realization the bed material distribution for each cell was randomly generated while satisfying the constraining conditions of equations (4) and (5). The mean and variance of the transport rates for all realizations was then estimated directly from the sequence of computed results. The key to a successful Monte Carlo simulation is a large number of realizations to ensure that the results are truly representative of the stochastic nature of the spatial heterogeneity.

[23] To examine the stochastic nature of the transport process, Wilcock and Crowe's original bedload transport model was employed in this study. It was assumed that the Wilcock and Crowe model is accurate for any given local GSD. Prior to the simulation, the flume bed was divided into n $\times$ m cells, covering a 4m reach upstream from the outlet. This was the portion of the flume used for the GSD sampling in the original experiment. In this study, n and m are taken as n = 40 and m = 6, resulting in 240 cells, each 0.1m $\times$ 0.1m. This configuration was selected because the largest particle size in the experiment was 5.38 cm, and it was assumed that approximately twice this scale was the impacted region of such a particle.

[24] To calculate the fractional transport rate in each cell, the local GSD was required. The distribution was obtained by counting the total particle number for each size fraction in one cell. This data was obtained by randomly placing each particle into one cell. The total particle number of each size fraction was calculated in advance. The particle random placing approach was used in this study rather than the probability density function approach because it is more general and more accurate. Because this method requires considerable computational resources for distributing small size particles, we used equation (9) and the procedures presented thereabout to generate the random field for the local GSD.

[25] The overall procedure used for conducting the Monte Carlo simulation for each of Wilcock's 47 experiments was as follows: (1) calculate the total particle number of each size fraction on the basis of the global GSD of an experimental run and the area of study domain, as described in section 2.1; (2) generate a random number between 1 and n $\times$ m for each particle in fractions of $d_i > 8$ mm to randomly place it in a cell and calculate the total particle number of each size fraction in each cell; (3) calculate the remaining volume for $d_i < 8$ mm in each volume and distribute the volume for each fraction using equation (9), assuming particles are spherical and the porosity is 0.3; (4) calculate the size composition in each cell on the basis of the total volume of each size fraction; (5) calculate the transport rate in each cell in row n (the last row before outlet) on the basis of the GSD calculated in step 4 and the flow condition in Wilcock's experimental data; (6) calculate the cross-sectional averaged transport rate at the flume outlet on the basis of the equation

$$\overline{W}_i \overline{P}_i = \sum_{k=1}^{m} W_{i,k} P_{i,k} \tag{15}$$

where $\overline{W}_i$ is the cross-sectional averaged transport rate for size fraction i and $\overline{P}_i = \frac{1}{m}\sum_{k=1}^{m} P_{i,k}$ is the cross-sectional averaged percentage of size fraction i; and (7) go back to step 2 and enter the next realization until 1000 realizations are finished.

[26] The Monte Carlo simulation does not exhaust all possibilities of the size composition in each cell. However, numerous realizations can effectively approximate the distribution of the particle size composition for the entire domain. Thus it is possible to demonstrate the significance of the uncertainty from a sufficiently large number of realizations.

[27] The hydraulic parameters specified in the simulations strictly followed the experiment measurements and were kept the same for all realizations within an experimental run. Also, shear stress distributions were adjusted for the side wall effect following the approach presented by *Wilcock et al.* [2001].

5. Results and Discussion

[28] In total, 1000 realizations were implemented for each experimental condition. Therefore, for each experimental run, 1000 possible transport rates for each size fraction were generated. Sample results of simulated transport rates, W_i, for several size fractions of selected experimental runs are shown in Figure 3. The transport rates are plotted on a logarithmic scale. Figure 3 shows that the logarithmic transport rate is a stochastic variable and it approximately satisfies the normal distribution.

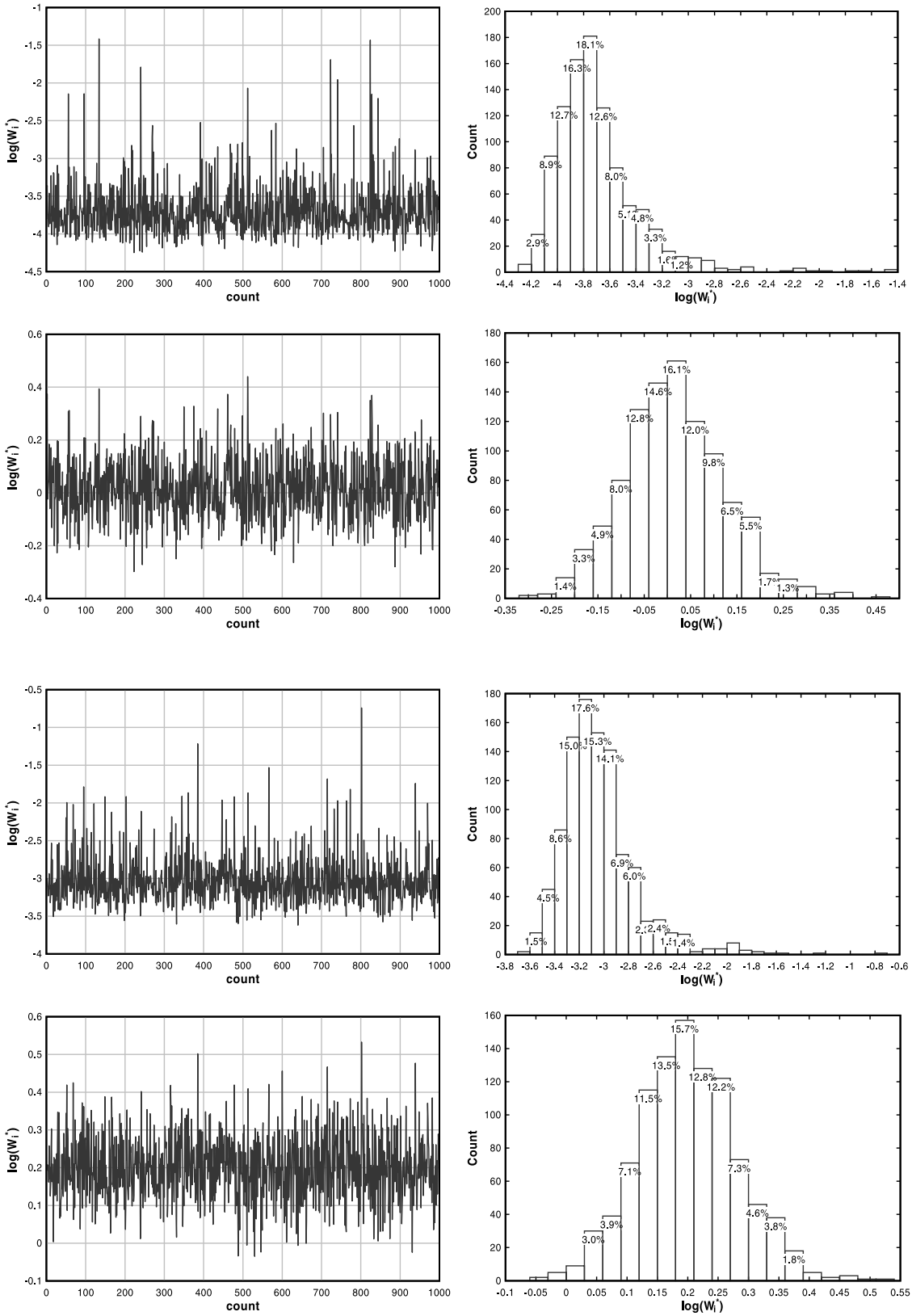

Figure 3. Example results of Monte Carlo simulations. (left) The 1000 simulated fractional transport rates (W_i) in log scale of each of the four arbitrarily selected cases and (right) the four corresponding distributions of the 1000 transport rates.

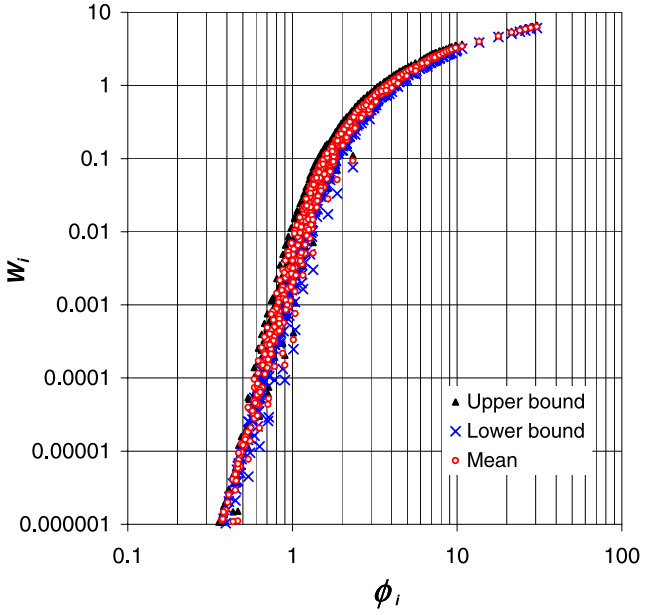

Figure 4. Monte Carlo simulation results of dimensionless fractional transport rate W_i against dimensionless shear stress φ_i for all of Wilcock's experiments. Each mean value is the averaged transport rate of 1000 realizations for a size fraction in one experiment. Upper/lower bounds are the mean ±1 standard deviation of the 1000 realizations.

[29] The simulated mean fractional transport rates and standard deviations from the 1000 realizations of each size fraction were calculated for each experimental run. The mean values and upper and lower bounds (defined here as 1 standard deviation from the mean) are shown in Figure 4. In this simulation, the equilibrium transport status was assumed and the local transport rate was determined by the flow condition and the local GSD. Practically, however, the local GSD and local transport rate change with time. Therefore each of the realizations in our simulation is analogous to an instant transport rate during an extended transport process. If the ergodic assumption is applicable, the mean value of all the realizations is close to the long time averaged transport rate. Figure 4 illustrates the variations in fractional transport rates among realizations. It also shows that the fractional transport rate has a large variance at low transport rates and less variance for high transport rates.

[30] The mean fractional transport rates of all realizations were calculated for each size fraction for each experimental run. Figure 5 shows the mean values of the Monte Carlo simulation results compared with Wilcock's experimental data and the deterministic transport equation, respectively. It is notable that the mean transport rates do not fall on one single-valued curve. Rather the data form a belt with the same trend as the observed data and the deterministic model. Significant transport rate uncertainty is evident from this result. The vertical belt width is larger than 1 order of magnitude at low transport rates. This result supports our speculation that the transport rate is a random variable due to the heterogeneous local GSD. The belt is wider at low transport rates and gradually contracts to a line at the high transport rate end. This trend shows that the mean transport rate has larger uncertainty at low shear stress or for coarse particles. Apparently, the uncertainty was reduced at very low transport rates. This is attributed to the fact that some of the simulation results were too low to be plotted in the given range. Also, the simulation was restricted by the limited number of experimental cases and there was very little data for the condition of low normalized shear stress.

[31] Additionally, the total transport rate of the mixture was modeled with the Monte Carlo simulation using the local geometric mean size in each cell. Again, 1000 realizations were simulated as shown in Figure 6. Figure 6 shows

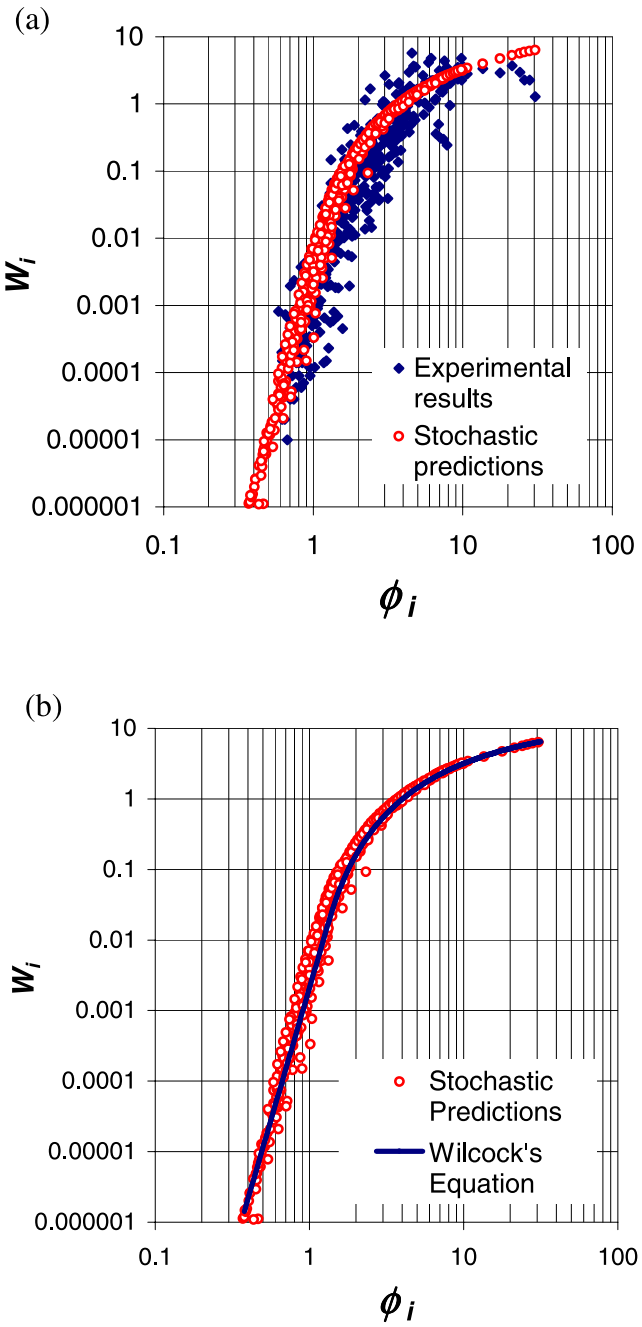

Figure 5. Comparison of Monte Carlo simulation results to (a) Wilcock's experimental data and (b) the Wilcock and Crowe equation. The stochastic predictions are the mean values of the Monte Carlo simulation.

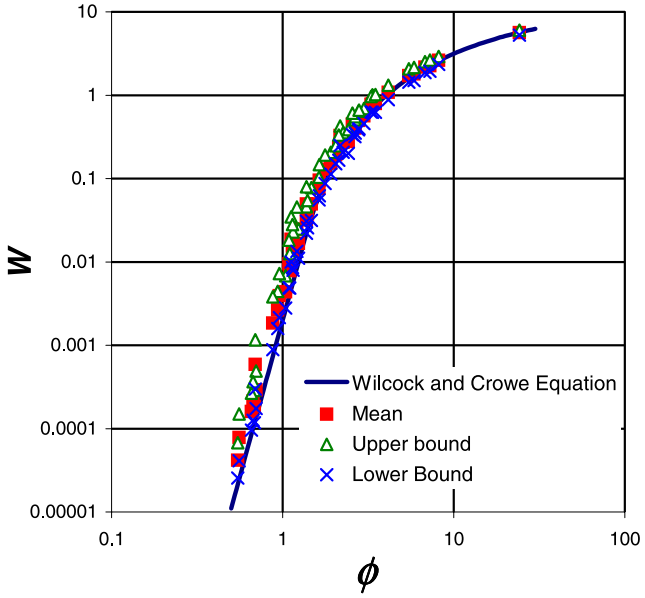

Figure 6. Monte Carlo Simulation results for the total transport rate. A mean value is the averaged total transport rate of the 1000 realizations. Upper/lower bounds are the mean ±1 standard deviation of the 1000 simulation results. All of Wilcock's 47 experiments are shown along with the Wilcock and Crowe equation.

that the total transport rates, calculated stochastically, were different from the original model, but they fell within a very narrow band. This was consistent with the observed total transport rate data, which also formed a much narrower band than the fractional transport rate. This implies that the total transport rate had less uncertainty than the fractional transport rate. It is notable that the stochastic results were always larger than the deterministic results.

[32] Figure 7 illustrates the variation of local GSDs generated with the random particle allocation approach in the Monte Carlo simulation. Using the simulation of experiment BOMC6 as an example, a histogram of the randomly generated local geometric mean size is plotted. To produce the histogram, the geometric mean sizes were counted for 1000 realizations in all 240 cells (i.e., 240,000 samples in total). The histogram shows that the local geometric mean size ranged from 1 mm to 37.5 mm, with a high probability of occurrence around the global geometric mean size of 2.64 mm. Some extreme situations that were characterized by large or small mean size did occur in the simulation but with very low frequency. This is consistent with the nature of well-mixed sediment.

[33] Two types of numerical experiments were conducted to examine the sensitivities of the transport rate uncertainty. The first experiment varied the flume width while holding the cell size constant. Figure 8a contains the results of a comparison between flume widths of 0.3 m, 0.6 m and 1.2 m with a cell size of 0.1 m × 0.1 m. The stochastically simulated transport rate W_i was normalized by the Wilcock and Crowe equation predicted value W_{oi}. Also, the results represent the mean transport rate of 1000 realizations. In this experiment, it was assumed that the global size distributions were the same for each case. When compared with the actual flume width of 0.6 m, the width of 0.3 m slightly increased the uncertainty while the 1.2 m width substantially reduced the uncertainty. The results indicate that the uncertainty is reduced with an increasing lateral scale. It is expected that the uncertainty will be reduced to a negligible level if the lateral scale is several orders of magnitude larger than L_{min}.

[34] The second experiment was to test the effect of variable cell sizes. A cell size of 0.1 m × 0.1 m was compared with a cell size 0.2 m × 0.2 m for a constant flume width of 0.6 m. A comparison of the two scenarios is plotted in Figure 8b. The results show that the uncertainty was reduced with a larger cell size. As the cell size is increased, the particle size distribution in the cell will tend to approach the global size distribution and differences between the cells are reduced. However, this may exaggerate the impact area of each particle and overestimate the hiding and exposing effect and therefore underestimate the uncertainty.

6. Implications to Field Situations

[35] The current study focused on an apparently well-mixed sediment mixture and found the existence of intrinsic

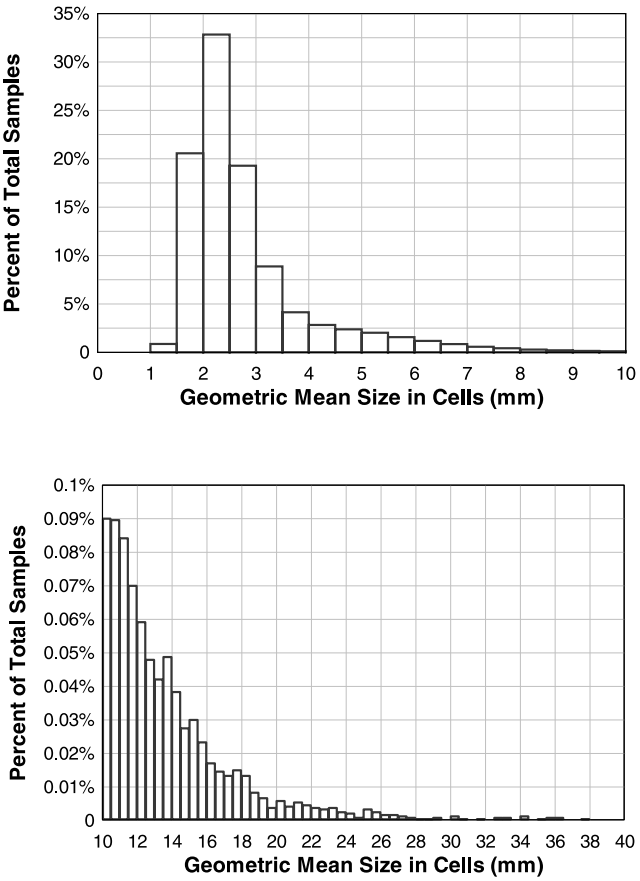

Figure 7. Example of the histogram of randomly generated local geometric mean size. Bed material from experiment BOMC6 provided the global grain size distribution, which had a global geometric mean size of 2.64 mm. The total sample population was 240,000 (240 cells by 1000 realizations). The local geometric mean size ranged from 1 to 37.5 mm, including some extreme situations with very low occurring frequency.

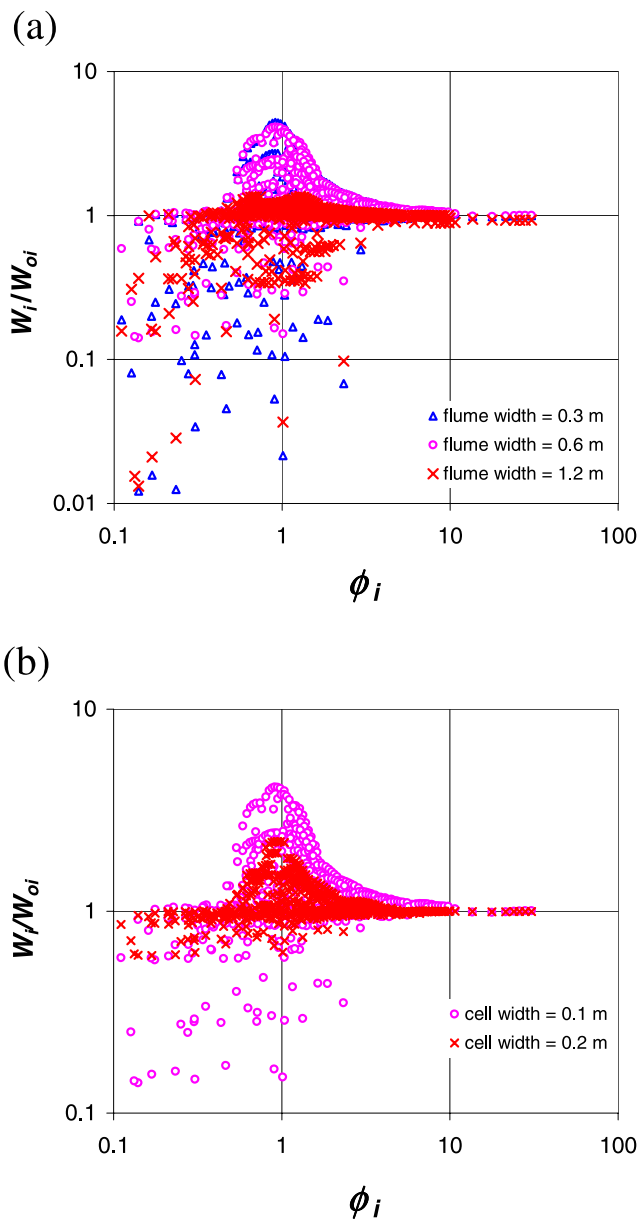

Figure 8. The dimensionless fractional transport rate (W_i) normalized by the prediction of the Wilcock and Crowe equation (W_{oi}) as a function of dimensionless shear stress (φ_i). (a) Two hypothetical flume widths (0.3 and 1.2 m) are tested to compare with the actual flume width (0.6 m). Cell sizes are fixed at 0.1 m. (b) The modeling results using two different cell sizes (0.1 and 0.2 m).

heterogeneity that may introduce significant uncertainty in the sediment transport prediction. In field situations, however, the sediment is generally not "well-mixed" because of hydrodynamic heterogeneity, stream geometry, and sediment sources. Hence the heterogeneity in field situations may be even greater than the intrinsic heterogeneity. The implication of the current study is that wherever heterogeneous sediment exists, it may introduce significant uncertainty into the transport prediction if only the global GSD is considered. In field applications, two-dimensional and three-dimensional sediment transport models may be able to accommodate the lateral (cross-sectional) variation of the GSD, but such models require descriptions of the initial conditions for the spatial distribution of the GSD. If this information is not available, an uncertainty analysis for the sediment transport rate may improve understanding of the deterministic predictions.

7. Conclusions

[36] The Monte Carlo simulation illustrates that the macroscale deterministic transport model is unable to reveal the uncertainty of the mixed size bedload transport process. From the simulation results the following conclusions are drawn.

[37] 1. The global GSD is not adequate for predicting the fractional bedload transport rate. The transport rate of gravel-sand mixtures corresponding to certain global GSD is essentially a stochastic variable. The uncertainty can be caused solely by the spatial heterogeneity of the local GSD.

[38] 2. The fractional transport rate can have significant uncertainty induced by a heterogeneous bed material, while the total transport rate has much less uncertainty. This is consistent with the experimental results.

[39] 3. The simulation results show that the uncertainty is increased as shear stress is reduced and as the grain size is increased.

[40] The bedload transport process is extremely complicated and it is related to many physical parameters and their interactions. This study examines just one of these many aspects. For example, questions still remain regarding the cause of uncertainty at high transport rates where the uncertainty associated with bed material heterogeneity is low. Such uncertainty is apparently a complex affect of multiple interacting factors.

[41] The work presented here has advanced our ability to quantify one of the many sources of uncertainty in estimates of sediment transport. Future research efforts in this area should expand focus on quantifying other sources of uncertainty and reducing uncertainty in sediment transport models.

[42] **Acknowledgments.** This research was supported by the U.S. Army Corp of Engineers under contract DACW42-03-2-0000. We would like to thank all reviewers for valuable comments that improved the quality of this manuscript.

References

Bagnold, R. (1966), An approach to the sediment transport problem from general physics, *Geol. Surv. Prof. Pap., 422-I.*

Bridge, J. S., and S. J. Bennett (1992), A model for the entrainment and transport of sediment grains of mixed sizes, shapes and densities, *Water Resour. Res.*, *28*, 337–363.

Bunte, K., and S. R. Abt (2001), Sampling surface and subsurface particle-size distributions in wadable gravel-and cobble-bed streams for analyses in sediment transport, hydraulics, and streambed monitoring, *Gen. Tech. Rep. RMRS-GTR-74*, 428 pp., For. Serv., Rocky Mt. Res. Stn., U. S. Dep. of Agric., Fort Collins, Colo.

Chien, N., and Z. Wan (1999), *Mechanics of Sediment Transport*, Am. Soc. of Civ. Eng., Reston, Va.

Einstein, H. (1950), The bed-load function for sediment transportation in open channel flow, *Tech. Bull. 1026*, U. S. Dep. of Agric., Washington, D. C.

Papanicolaou, A. N., P. Diplas, C. L. Dancey, and M. Balakrishnan (2001), Surface roughness effects in near-bed turbulence: Implications to sediment entrainment, *J. Eng. Mech.*, *127*, 211–218.

Parker, G. (1990), Surface-based bedload transport relation for gravel rivers, *J. Hydraul. Res.*, *28*, 417–436.

Parker, G., P. C. Klingeman, and D. L. McLean (1982), Bedload and size distribution in paved gravel-bed streams, *J. Hydraul. Eng.*, *108*, 544–571.

Seal, R., and C. Paola (1995), Observations of downstream fining on the North Fork Toutle River near Mount St. Helens, Washington, *Water Resour. Res.*, *31*, 1409–1419.

Stone, M. C., and R. H. Hotchkiss (2007a), Evaluating ADCP velocity, shear stress, and turbulence measurements in two cobble bed rivers, *J. Hydraul. Res.*, *45*, 752–762.

Stone, M. C., and R. H. Hotchkiss (2007b), Turbulence descriptions in two cobble-bed river reaches, *J. Hydraul. Eng.*, *133*, 1367–1378.

Wiberg, P. L., and J. D. Smith (1989), Model for calculating bed load transport of sediment, *J. Hydraul. Eng.*, *115*, 101–123.

Wilcock, P. R., and J. C. Crowe (2003), Surface-based transport model for mixed-size sediment, *J. Hydraul. Eng.*, *129*, 120–128.

Wilcock, P. R., and B. W. McArdell (1993), Surface-based fractional transport rates: Mobilization thresholds and partial transport of a sand-gravel sediment, *Water Resour. Res.*, *29*, 1297–1312.

Wilcock, P. R., S. T. Kenworthy, and J. C. Crowe (2001), Experimental study of the transport of mixed sand and gravel, *Water Resour. Res.*, *37*, 3349–3358.

Wu, F., and M. Jiang (2007), Numerical investigation of the role of turbulent bursting in sediment entrainment, *J. Hydraul. Eng.*, *133*, 329–334.

Yalin, M. S. (1977), *Mechanics of Sediment Transport*, Pergamon, New York.

L. Chen and M. C. Stone, Division of Hydrologic Sciences, Desert Research Institute, Las Vegas, NV 89119, USA. (lchen@dri.edu)